Modeling and Parameter Identification of an Active Anti-Vibration System

Brad M. Beadle*, Stefan Hurlebaus*, Uwe Stöbener**, Lothar Gaul*
* Institute A of Mechanics, University of Stuttgart, Allmandring 5 b,
70550 Stuttgart, Germany
**Halcyonics GmbH, Tuchmacherweg 12, 37079 Göttingen, Germany

ABSTRACT

In the fields of high-resolution metrology and manufacturing, effective anti-vibration measures are required to obtain precise and repeatable results. This is particularly true when the amplitudes of ambient vibration and the dimensions of the investigated or manufactured structure are comparable, e.g. in sub-micron semiconductor chip production, holographic interferometry, confocal optical imaging, and scanning probe microscopy. In the active anti-vibration system examined, signals are acquired by extremely sensitive vibration detectors, and the vibration is reduced using a feedback controller to drive electrodynamic actuators. This paper deals with the modeling of this anti-vibration system. First, a six-degree-of-freedom rigid body model of the system is developed. The unknown parameters of the unloaded system, including actuator transduction constants, spring stiffness, damping, moments of inertia, and the location of the center of mass, are determined by comparing measured transfer functions to those calculated using the updated model. The model is then re-updated for the case of an arbitrarily loaded system. The responses predicted by the final updated model agree well with the experimental measurements, thereby giving confidence in the model and the updating procedure.

Keywords: Active vibration isolation, model updating, parameter identification, six-degree-of-freedom rigid body

1. INTRODUCTION

Isolating a piece of delicate equipment from the vibration of a base structure is of practical importance in a number of engineering fields. The quest for tighter production tolerance and higher resolution has led to more stringent requirements regarding ambient vibration levels. In the majority of cases, the base supporting a piece of precision equipment is flexible and vibrates with an unpredictable waveform containing significant energy over a fairly broad range of frequencies. The active isolation of equipment from a vibrating base structure is considered in this paper. Passive anti-vibration mounts are widely used to isolate precision equipment from base vibration. Although conventional passive mounts offer good isolation at high frequencies, they suffer from vibration amplification at the mounted resonance frequency. Generally, the best isolation performance is achieved by using an active system in combination with a passive mount, whereby the fundamental mounted resonance can be actively controlled without compromising the high frequency performance.

A good overview of active vibration isolation techniques can be found in the text written by Fuller, et al. [1]. Various control strategies are discussed, including feedforward and feedback concepts for systems which vibrate periodically or randomly. Stöbener, Gaul [2] and Hurlebaus [3] modeled a piezoelectric stack actuator with finite elements and investigated the response of a one-degree-of-freedom (DOF) vibration isolation system having such a stack actuator built in. In addition, feedforward and feedback control techniques for enhancing the isolation effect were investigated. Huang, et al. [4] presented a theoretical and experimental investigation of an active vibration isolation system. In that study, a decentralized velocity feedback controller was implemented in which individual actuators were separately controlled by using the velocity measured at the actuator location as feedback. This control method was found to be effective and robust for multichannel control systems. Riebe and Ulbrich [5] presented a model for a six-DOF robot arm. A physical model describing the frictional behavior was developed, and the friction model parameters were experimentally identified. Furthermore, a comparison between measured and simulated actuation forces was made.

This paper investigates a commercially available six-DOF active vibration isolation system. Fig. 1 depicts the examined vibration isolation system. Active vibration isolation is achieved in the as-built system using a decentralized analog velocity feedback "SISO" (single input, single output) controller. The ultimate goal of the study is to investigate alternative controllers, such as a MIMO (multiple input, multiple output) controller, for use in vibration isolation. However, successful implementation of such controllers first requires an accurate physical model of the vibration isolation system. In section 2, a six-DOF rigid body model of the vibration isolation system is developed. In section 3, model parameters associated with the unloaded and loaded isolation system are determined using experimentally measured transfer functions.

Fig.1: Commercially available active vibration isolation system.

2. MODELING

2.1. Physical Model of the Vibration Isolation System

The vibration isolation system is essentially composed of two plates connected by springs and actuators. Physical models of the vibration isolation system are depicted in figs. 2 and 3. Fig. 2 depicts a physical model of the upper plate, and fig. 3 depicts the overall vibration isolation system for an arbitrary loading. Assuming that the motion of the upper plate undergoes rigid body motion only, then its motion can be described using six coordinates. Referring to the upper plate, the coordinates x, y, and z are used to describe the linear motion of the plate, and the coordinates ϕ_x, ϕ_y, and ϕ_z describe small rotations about the x, y, and z axes, respectively. The coordinate system is located at the center of mass of the plate. Due to plate symmetry, the x and y coordinates of the center of mass coincide with the geometric center of the plate. Similarly, the motion of the lower plate is described using the coordinates x^d, y^d, z^d, $\phi_x{}^d$, $\phi_y{}^d$, and $\phi_z{}^d$.

The upper plate is suspended above the lower plate with four springs, each of which is denoted by the vertical stiffness k_s. The physical model contains additional stiffnesses, namely k_t and k_r, to model the transverse and rotational stiffness, respectively, associated with the suspension springs. Presumably, the motion of the lower plate is identical to the motion of the surface upon which the vibration isolation system rests. The coordinates describing the motion of the lower plate can therefore be viewed as *disturbance* inputs. The motion of the lower plate is then coupled to the upper plate via the suspension, transverse, and rotational springs. Four vertical actuators, A_1-A_4, and four horizontal actuators, A_5-A_8, are rigidly attached to the upper plate, and interact with the lower plate via point contact. The vertical actuators can slide horizontally relative to the lower plate, and the horizontal actuators can slide vertically relative to the lower plate. Active vibration control is realized by driving the actuators with the appropriate control inputs. The coordinates L_1-L_3 are used to locate the suspension springs and the vertical actuators. The coordinates L_4-L_6 are used to locate the horizontal actuators. Finally, the coordinates L_7-L_9 are used to locate the center of mass of the supported equipment relative to the center of mass of the upper plate.

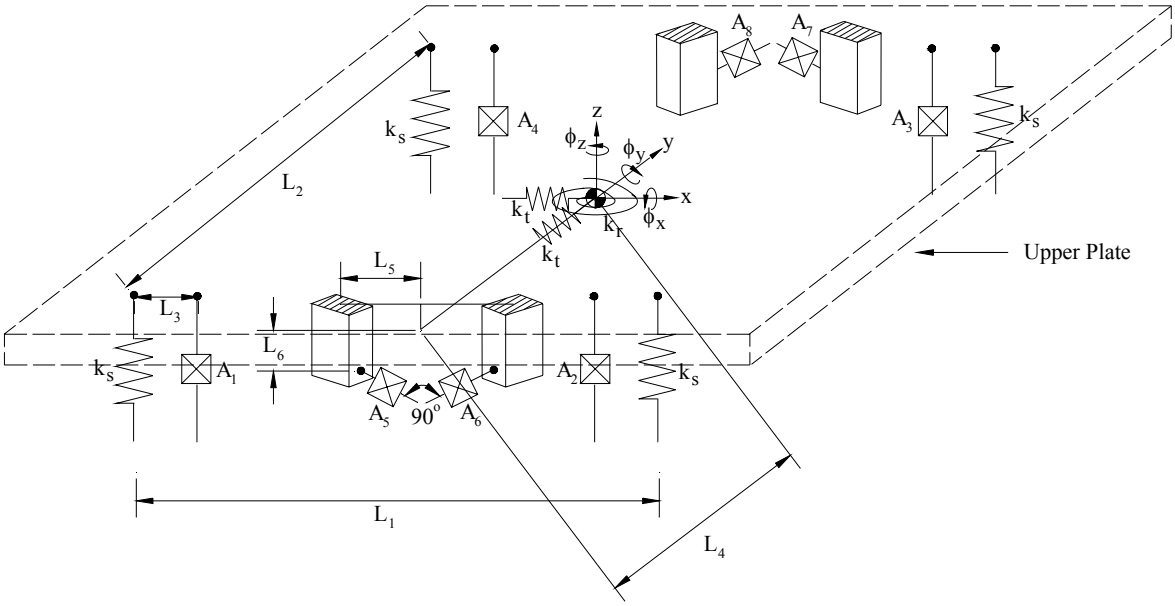

Fig.2: Physical model of the unloaded vibration isolation system.

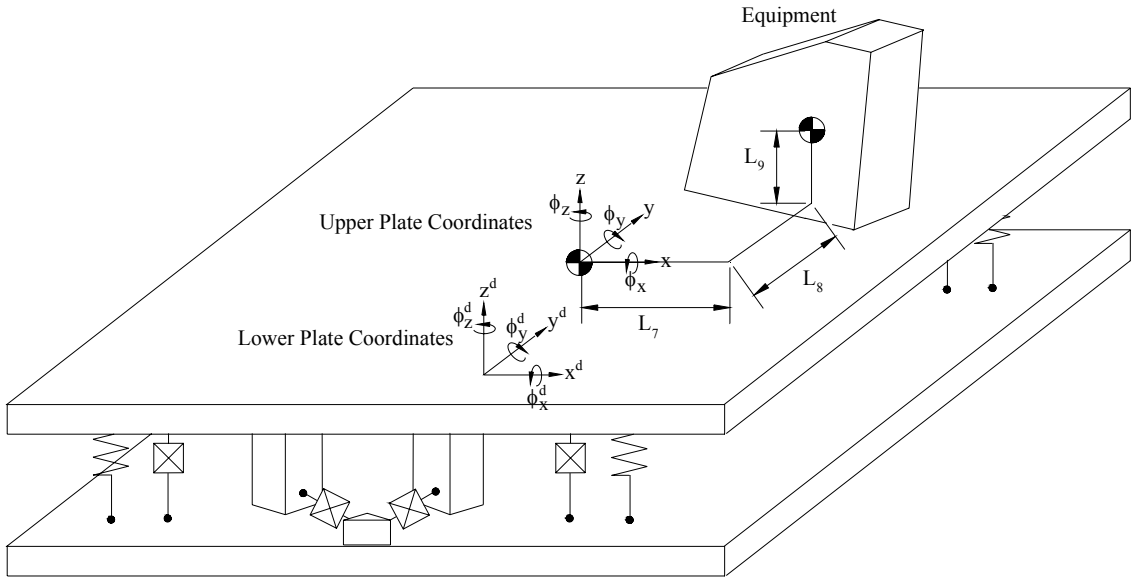

Fig.3: Physical model of the loaded vibration isolation system.

2.2. Physical Model of an Actuator

The physical model of an actuator is depicted in fig. 4. The main components of the actuator are a stationary permanent magnet and a coil-wrapped reaction mass m_a which moves relative to the permanent magnet. A damper having value d_a has been included to model energy losses, and a spring having stiffness k_a has been included to model the spring-like restoring force between the permanent magnet and the reaction mass. When a voltage V is applied to the coil, a current I will flow through it. Assuming that the coil is purely resistive, the current and voltage are related by Ohm's law, $V = IR$, where R is the resistance of the coil. An electromotive force F proportional to the current, and therefore to the applied voltage, is developed by the coil, thereby causing the reaction mass to accelerate. The equation of motion of the reaction mass is given by

$$m_a \ddot{x} + d_a \dot{x} + k_a = F = eV \,, \tag{1}$$

where e (units N/V) is an actuation constant which relates the applied voltage to the electromotive force developed.

Fig. 5 depicts the theoretical and measured displacement-force (X/F) transfer function for a freely vibrating actuator. The reaction mass was measured to be m_a = 0.05 kg using a mass scale. The parameter set which yielded the smallest least-squares error between the theoretical and experimental X/F transfer functions was determined to be d_a = 7.1 Nm/s, k_a = 7300 N/m, and e = 0.39 N/V.

A simplified actuator model is depicted to the right in fig. 4. This is the actuator model which will be implemented in the model for the vibration isolation system. The reaction mass has been eliminated in the simple model since its motion is totally constrained in the vibration isolation system. Additionally, the damping parameter has been left out, since its effects are negligible in comparison to other energy loss mechanisms, such as the friction occurring at the points of contact between the lower plate and the actuators.

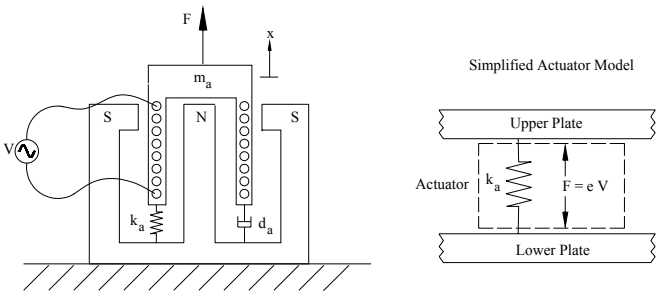

Fig.4: Physical model of an actuator.

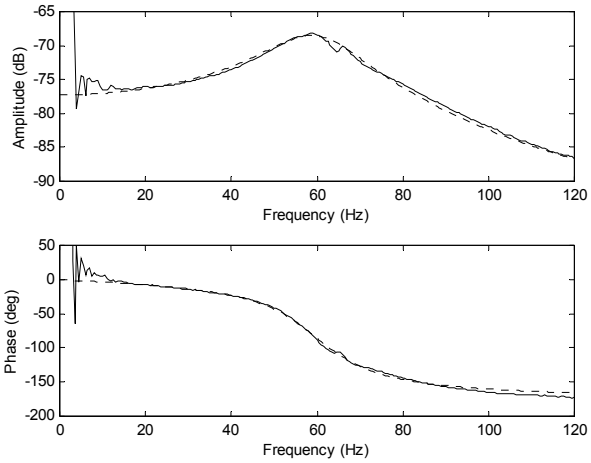

Fig. 5: Experimental (solid) and theoretical (dashed) X/F transfer functions for a freely-vibrating actuator.

2.3. Equations of Motion for the Loaded Vibration Isolation System

The equations of motion for a system composed of j rigid bodies are [6]

$$\sum \overline{F} = \sum_j m_j \left(\overline{a}_{Gj}\right) \tag{2}$$

$$\sum \overline{M}_P = \sum_j \dot{\overline{H}}_{Gj} + \sum_j \left[\overline{r}_{Gj/P} \times m_j \left(\overline{a}_{Gj}\right)\right]. \tag{3}$$

Eqn. 2 is the overall system force balance, with m_j being the mass of the jth rigid body and with $\overline{a}_{Gj}$ being the acceleration of the jth rigid body's center of mass. Eqn. 3 is the overall moment balance about an arbitrary point P, with $\dot{\overline{H}}_{Gj}$ being the rate of change of angular momentum about the center of mass for the jth rigid body and with $\overline{r}_{Gj/P}$ being the position vector of the jth rigid body's center of mass relative to the point P. The vibration isolation system is composed of 3 rigid bodies: the lower plate, the upper plate, and the equipment resting on top of the upper plate. The motion of the lower plate is presumably given, i.e., it has the same motion as the surface upon which it rests. Eqns. 2 and 3 can then be used to solve for the unknown motion of the upper plate and the equipment.

The mass of the upper plate is defined as m, and the mass of the equipment is defined as m_e. Additionally, the acceleration $\ddot{\bar{x}}_e$ of the equipment's center of mass can be related to the acceleration $\ddot{\bar{x}}$ of the upper plate's center of mass by

$$\ddot{\bar{x}}_e = \ddot{\bar{x}} + \ddot{\bar{\phi}} \times \bar{r}_e + \dot{\bar{\phi}} \times \left(\dot{\bar{\phi}} \times \bar{r}_e \right), \tag{4}$$

where

$$\bar{x} = \left\{ x \quad y \quad z \right\}^{\mathrm{T}}, \tag{5}$$

$$\bar{\phi} = \left\{ \phi_x \quad \phi_y \quad \phi_z \right\}^{\mathrm{T}}, \tag{6}$$

and

$$\bar{r}_e = \left\{ L_7 \quad L_8 \quad L_9 \right\}^{\mathrm{T}}. \tag{7}$$

Assuming that the angular displacement of the upper plate is small, then the third term on the right hand side of eqn. 4 may be neglected. Using eqn. 4, eqn. 2 may be rewritten as

$$\sum \bar{F} = \left(m + m_e \right) \ddot{\bar{x}} + m_e \left(\ddot{\bar{\phi}} \times \bar{r}_e \right) \tag{8}$$

Eqn. 3 can be simplified by performing the moment balance about the upper plate's center of mass:

$$\sum \bar{M} = \dot{\bar{H}} + \dot{\bar{H}}_e + \bar{r}_e \times m_e \left(\ddot{\bar{x}} + \ddot{\bar{\phi}} \times \bar{r}_e \right), \tag{9}$$

where $\dot{\bar{H}}$ and $\dot{\bar{H}}_e$ are the rates of change of angular momentum for the upper plate and equipment, respectively. The rate of change of the upper plate's angular momentum can be expressed as

$$\dot{\bar{H}} = [I] \ddot{\bar{\phi}} + \dot{\bar{\phi}} \times \left([I] \dot{\bar{\phi}} \right). \tag{10}$$

In the above equation, [I] is the inertia matrix, and it has the general form

$$[I] = \begin{bmatrix} I_{xx} & -I_{xy} & -I_{xz} \\ -I_{xy} & I_{yy} & -I_{yz} \\ -I_{xz} & -I_{yz} & I_{zz} \end{bmatrix}. \tag{11}$$

Since the coordinate system for the upper plate is aligned with the principal axes, then the inertia matrix has only diagonal entries. Additionally, assuming that the angular displacement of the upper plate is small, then the second term on the right hand side of eqn. 10 may be neglected. With these simplifications, the rate of change of the upper plate's angular momentum becomes

$$\dot{\bar{H}} = \left\{ I_{xx} \ddot{\phi}_x \quad I_{yy} \ddot{\phi}_y \quad I_{zz} \ddot{\phi}_z \right\}^{\mathrm{T}}. \tag{12}$$

The rate of change of the equipment's angular momentum is given by

$$\dot{\bar{H}}_e = \left[I^e \right] \ddot{\bar{\phi}}. \tag{13}$$

Because the chosen coordinate system does not necessarily align with the equipment's principal axes, then the inertia matrix $[I_e]$ will have the general form given in eqn. 11. Substituting eqns. 12 and 13 into eqn. 9 yields the final expression for the moment balance,

$$\sum \overline{M} = \begin{bmatrix} I_{xx} + I_{xx}^{\,e} & -I_{xy}^{\,e} & -I_{xz}^{\,e} \\ -I_{xy}^{\,e} & I_{yy} + I_{yy}^{\,e} & -I_{yz}^{\,e} \\ -I_{xz}^{\,e} & -I_{yz}^{\,e} & I_{zz} + I_{zz}^{\,e} \end{bmatrix} \ddot{\overline{\phi}} + \overline{r}_e \times m_e \left(\ddot{\overline{x}} + \ddot{\overline{\phi}} \times \overline{r}_e \right). \tag{14}$$

The left hand side of eqn. 8 is determined by summing force contributions from the various springs and the actuators. Similarly, the left hand side of eqn. 14 is determined by summing the moment contributions from the springs and actuators about the upper plate's center of mass. Müller, et. al [7] determine in detail the force and moment contributions from the springs and actuators attached to a three-DOF rigid body system. Eqns. 8 and 14 can then be rearranged into a convenient set of equations which describe the motion of the loaded upper plate:

$$[M]\ddot{\overline{w}} + [D]\dot{\overline{w}} + [K]\overline{w} = [D]\dot{\overline{w}}^{d} + [K]\overline{w}^{d} + [E]\overline{v}\,, \tag{15}$$

where

$$[M] = \begin{bmatrix} m+m_e & 0 & 0 & 0 & m_e L_9 & -m_e L_8 \\ 0 & m+m_e & 0 & -m_e L_9 & 0 & m_e L_7 \\ 0 & 0 & m+m_e & m_e L_8 & -m_e L_7 & 0 \\ 0 & -m_e L_9 & m_e L_8 & I_{xx} + I_{xx}^{\,e} + m_e\left(L_8^{\,2} + L_9^{\,2}\right) & -I_{xy}^{\,e} - m_e L_7 L_8 & -I_{xz}^{\,e} - m_e L_7 L_9 \\ m_e L_9 & 0 & -m_e L_7 & -I_{xy}^{\,e} - m_e L_7 L_8 & I_{yy} + I_{yy}^{\,e} + m_e\left(L_7^{\,2} + L_9^{\,2}\right) & -I_{yz}^{\,e} - m_e L_8 L_9 \\ -m_e L_8 & m_e L_7 & 0 & -I_{xz}^{\,e} - m_e L_7 L_9 & -I_{yz}^{\,e} - m_e L_8 L_9 & I_{zz} + I_{zz}^{\,e} + m_e\left(L_7^{\,2} + L_8^{\,2}\right) \end{bmatrix}, \tag{16}$$

$$[D] = \begin{bmatrix} d_1 & 0 & 0 & 0 & 0 & 0 \\ 0 & d_1 & 0 & 0 & 0 & 0 \\ 0 & 0 & d_3 & 0 & 0 & 0 \\ 0 & 0 & 0 & d_4 & 0 & 0 \\ 0 & 0 & 0 & 0 & d_5 & 0 \\ 0 & 0 & 0 & 0 & 0 & d_6 \end{bmatrix}, \tag{17}$$

$$[K] = \begin{bmatrix} 2k_a + k_t & 0 & 0 & 0 & -2k_a L_6 & 0 \\ 0 & 2k_a + k_t & 0 & 2k_a L_6 & 0 & 0 \\ 0 & 0 & 4(k_a + k_s) & 0 & 0 & 0 \\ 0 & 2k_a L_6 & 0 & (k_a + k_s) L_2^{\,2} + 2k_a L_6^{\,2} & 0 & 0 \\ -2k_a L_6 & 0 & 0 & 0 & k_a\left[(L_1 - 2L_3)^2 + 2L_6^{\,2}\right] + k_s L_1^{\,2} & 0 \\ 0 & 0 & 0 & 0 & 0 & 2k_a (L_4 + L_5)^2 + k_r \end{bmatrix}, \tag{18}$$

$$[E] = \begin{bmatrix} 0 & 0 & 0 & 0 & -\frac{1}{\sqrt{2}}e_5 & \frac{1}{\sqrt{2}}e_6 & \frac{1}{\sqrt{2}}e_7 & -\frac{1}{\sqrt{2}}e_8 \\ 0 & 0 & 0 & 0 & \frac{1}{\sqrt{2}}e_5 & \frac{1}{\sqrt{2}}e_6 & -\frac{1}{\sqrt{2}}e_7 & -\frac{1}{\sqrt{2}}e_8 \\ e_1 & e_2 & e_3 & e_4 & 0 & 0 & 0 & 0 \\ -\frac{L_2}{2}e_1 & -\frac{L_2}{2}e_2 & \frac{L_2}{2}e_3 & \frac{L_2}{2}e_4 & \frac{L_6}{\sqrt{2}}e_5 & \frac{L_6}{\sqrt{2}}e_6 & -\frac{L_6}{\sqrt{2}}e_7 & -\frac{L_6}{\sqrt{2}}e_8 \\ -\left(L_3 - \frac{L_1}{2}\right)e_1 & \left(L_3 - \frac{L_1}{2}\right)e_2 & \left(L_3 - \frac{L_1}{2}\right)e_3 & -\left(L_3 - \frac{L_1}{2}\right)e_4 & \frac{L_6}{\sqrt{2}}e_5 & -\frac{L_6}{\sqrt{2}}e_6 & -\frac{L_6}{\sqrt{2}}e_7 & \frac{L_6}{\sqrt{2}}e_8 \\ 0 & 0 & 0 & 0 & -\frac{L_4 + L_5}{\sqrt{2}}e_5 & \frac{L_4 + L_5}{\sqrt{2}}e_6 & -\frac{L_4 + L_5}{\sqrt{2}}e_7 & \frac{L_4 + L_5}{\sqrt{2}}e_8 \end{bmatrix}, \tag{19}$$

$$\overline{w} = \begin{Bmatrix} x & y & z & \phi_x & \phi_y & \phi_z \end{Bmatrix}^{\mathrm{T}}, \tag{20}$$

$$\overline{w}^d = \begin{Bmatrix} x^d & y^d & z^d & \phi_x{}^d & \phi_y{}^d & \phi_z{}^d \end{Bmatrix}^{\mathrm{T}}, \tag{21}$$

and $\overline{v}$ is the matrix containing the input voltages applied to the respective actuators. The diagonal form of the damping matrix [*D*] assumes that the damping of a particular rigid body mode does not depend on the motion of another rigid body mode. The individual entries of the damping matrix are determined experimentally. The first two terms on the right hand side of eqn. 15 represent the disturbance excitation due to the motion of the lower plate. The third term on the right hand side of eqn. 15 is the excitation generated by the actuators. Finally, the form of the transducer coupling matrix [*E*] assumes that each actuator has a distinct transduction coefficient e_i.

Assuming that the disturbance inputs to the vibration isolation system are zero, $\overline{w}^d = 0$ (i.e., the bottom plate does not move), then eqn. 15 becomes

$$[M]\ddot{\overline{w}} + [D]\dot{\overline{w}} + [K]\overline{w} = [E]\overline{v}. \tag{22}$$

For the case of harmonic excitation, $\overline{v} = \overline{V}e^{i\omega t}$, the steady-state motion of the upper plate will also be harmonic, $\overline{w} = \overline{W}e^{i\omega t}$, so that eqn. 22 becomes

$$[G]\overline{W} = [E]\overline{V}, \tag{23}$$

where

$$[G] = -\omega^2[M] + i\omega[D] + [K]. \tag{24}$$

The solution to Eqn. 24 is given by

$$\overline{W} = [G]^{-1}[E]\overline{V}. \tag{25}$$

Assuming that the transducers being driven are identically excited, then $\overline{V}$ can be written as the product of an actuation vector $\overline{A}$ and a complex-valued voltage coefficient V_o,

$$\overline{V} = V_o\overline{A}. \tag{26}$$

The entries of the actuation vector are 0 or 1, depending on which actuators are being driven. Eqns. 25 and 26 together then give the displacement-voltage transfer function vector

$$\frac{\overline{W}}{V_o} = [G]^{-1}[E]\overline{A} \tag{27}$$

Following the definition of $\overline{w}$ in eqn. 20, $\overline{W}$ can be decomposed as

$$\overline{W} = \begin{Bmatrix} \overline{X} & \overline{\Phi} \end{Bmatrix}^{\mathrm{T}}. \tag{28}$$

The use of the filtering matrices $[F_X]$ and $[F_\Phi]$ allows the extraction of the partitioned vectors from eqn. 28:

$$\overline{X} = [F_X]\overline{W}, \quad [F_X] = \begin{bmatrix} 1 & 0 & 0 & 0 & 0 & 0 \\ 0 & 1 & 0 & 0 & 0 & 0 \\ 0 & 0 & 1 & 0 & 0 & 0 \end{bmatrix}, \tag{29}$$

$$\overline{\Phi} = [F_\Phi]\overline{W}, \quad [F_\Phi] = \begin{bmatrix} 0 & 0 & 0 & 1 & 0 & 0 \\ 0 & 0 & 0 & 0 & 1 & 0 \\ 0 & 0 & 0 & 0 & 0 & 1 \end{bmatrix}. \tag{30}$$

The complex displacement of an arbitrary point p in an arbitrary direction $\overline{s}$ can be expressed as

$$X_{ps} = \left(\overline{X} + \overline{\Phi} \times \overline{r}_p\right) \cdot \frac{\overline{s}}{|\overline{s}|}, \tag{31}$$

where $\overline{r}_p$ is the position vector of point p relative to the upper plate's mass center. It follows from eqns. 27, 29-31 that the transfer function between this displacement and the force developed by the rth actuator is

$$\frac{X_{ps}}{F_r} = \left[[F_X][G]^{-1}[E]\overline{A} + \left([F_\Phi][G]^{-1}[E]\overline{A}\right) \times \overline{r}_p\right] \cdot \frac{\overline{s}}{e_r|\overline{s}|}, \tag{32}$$

where e_r is the actuator constant for the rth actuator.

3. PARAMETER IDENTIFICATION

3.1. Experimental Setup

The experimental setup for identifying the unknown parameters in the theoretical model is depicted in fig. 6. The unknown parameters include spring stiffness, damping, actuator transduction constants, moments and products of inertia, and the location of the center of mass for both the upper plate and the equipment. The other constants required for the model are known: L_1=0.348 m, L_2=0.3 m, L_3=0.55 m, L_4+ L_5=0.19 m, and m =19.3 kg. In practice, it can be assumed that the equipment mass m_e will also be known. An HP Paragon measurement system is configured to drive one or more of the actuators using a random voltage excitation V. The excitation signal is amplified using the preamplifiers which are built into the commercial vibration isolation system. In the diagram, the vertical actuators are denoted by A_1-A_4, and the horizontal actuators are denoted by A_5-A_8. The response of the upper plate is measured using an accelerometer (Brüel & Kjær 4381) placed at one of the three measurement locations M_1-M_3. The commercial vibration isolation system actually has built-in accelerometers at each of the actuator locations. In future work, these accelerometers will be used for the parameter identification procedure. The commercial accelerometer used in the current study can be oriented to measure acceleration in any of the three coordinate directions. The acceleration signal is converted into displacement X using a signal conditioner before being received by the measurement system. The measurement system then computes the X/V transfer function from the random displacement and voltage waveforms. Division of the measured X/V transfer function by the appropriate actuator constant e_r results in the displacement-force transfer function X/F.

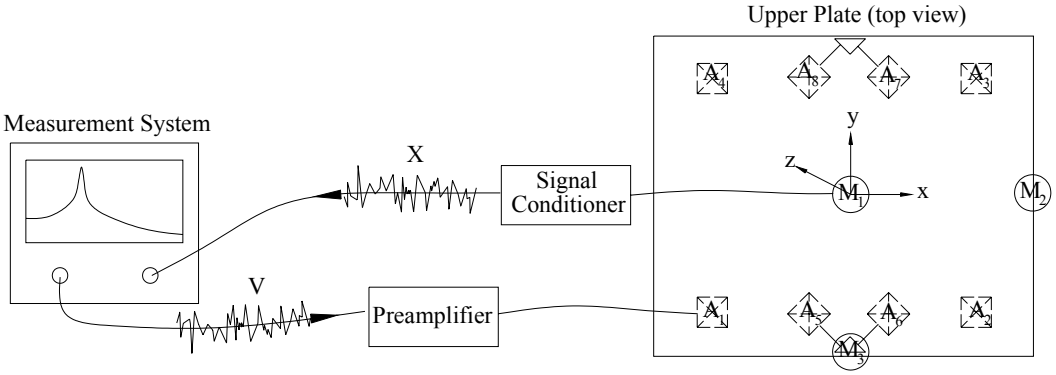

Fig. 6: Experimental setup for determining model parameters.

3.2. Unloaded Vibration Isolation System

The results of the parameter identification procedure for the unloaded vibration isolation system are summarized in Table 1. In test 5 for example, the four actuators A_1-A_4 were driven, and the accelerometer was used to measure the motion in the z-direction at measurement location M_3. Actuators A_3 and A_4 were driven 180° out of phase relative to actuators A_1 and A_2. This excitation scheme was not physically implemented, but instead, the transfer functions for two drive cases were subtracted. This particular drive scheme excites pure rotational motion about the x axis. Hence, the unknown moment of inertia and rotational damping about this axis can be determined by comparing the measured transfer function with the theoretical transfer function. Specifically, the theoretical transfer function Z_3/F_1 is computed using eqn. 32 for several different values of I_{xx} and d_4. An error function given by

$$error = \left(\overline{T}_{\text{exp}} - \overline{T}_{\text{theo}}\right) \cdot \left(\overline{T}_{\text{exp}} - \overline{T}_{\text{theo}}\right)^{*} \tag{33}$$

is then calculated, where $\overline{T}_{\text{exp}}$ and $\overline{T}_{\text{theo}}$ are the experimental and theoretical transfer functions, respectively, and the * operator denotes complex conjugation. The error function is calculated for values of the transfer functions in the frequency range 2.5-20 Hz. Finally, the parameter values which minimize the error function are determined.

Test	Actuator	Displacement	Parameter
1	A_1	z_1	e_1 = 6.59 N/V |
2	A_2	z_1	e_2 = 7.85 N/V | k_s=11300 N/m
3	A_3	z_1	e_3 = 7.07 N/V | d_3=275 Ns/m
4	A_4	z_1	e_4 = 8.10 N/V |
5	(A_1+ A_2)- (A_3+ A_4)	z_3	I_{xx}=0.340 kgm^2, d_4=6.74 Ns/rad
6	(A_1+ A_4)- (A_2+ A_3)	z_2	I_{yy}=0.259 kgm^2, d_5=3.48 Ns/rad
7	(A_1+ A_4)- (A_2+ A_3)	x_1	L_6=0.054 m
8	A_5	x_1	e_5 = 7.50 N/V |
9	A_6	x_1	e_6 = 7.89 N/V | k_t=37600 N/m
10	A_7	x_1	e_7 = 6.65 N/V | d_1=275 Ns/m
11	A_8	x_1	e_8 = 5.97 N/V |
12	A_5+ A_7	x_3	I_{zz}=0.500 kgm^2, k_r=1590 N/rad d_6=9.32 Ns/rad

Table 1: Parameter identification results for the unloaded vibration isolation system.

3.3. Loaded Vibration Isolation System

An automatic parameter identification procedure has been developed for the case of arbitrary loading. The convergence and accuracy of the procedure was tested for the particular loading case depicted in fig. 7. The location of the center of mass and the moments & products of inertia for this particular loading are summarized in table 2 in the column labeled "actual value". Since the z coordinate axis is aligned with the load's principal vertical axis, the products of inertia I_{xz} and I_{yz} are zero. In practice, the z coordinate axis will usually coincide with the load's vertical principal axis. However, for the case in which none of the coordinate axes aligns with the load's principal axes, a procedure similar to that used to determine I_{xy} here, can be used to determine all products of inertia.

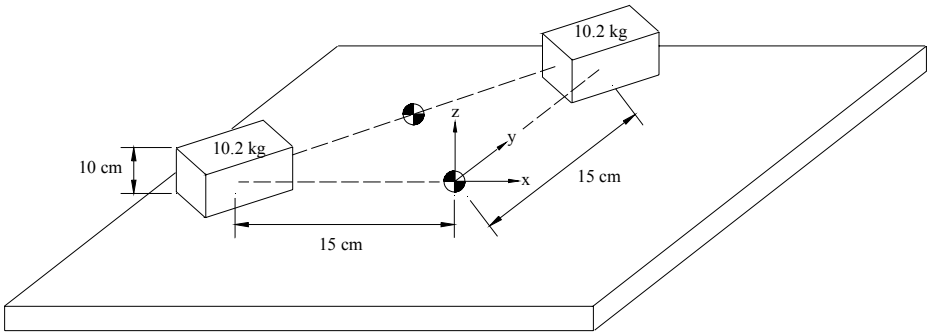

Fig. 7: Loading case used to verify the parameter identification procedure.

The results of the parameter identification procedure are contained in table 2. It has been assumed that the previously determined actuator constants e_1-e_8 and damping coefficients d_1-d_6 remain unaffected by the loading, and therefore do not need to be identified. For explanation purposes, consider test 4, which is used to determine the total moment of inertia $I_{xx} + I_{xx}^{e}$. As in the unloaded case, four actuators A_1-A_4 were driven, and the accelerometer was used to measure the motion in the z-direction at measurement location M_3. Actuators A_3 and A_4 were driven 180° out of phase relative to actuators A_1 and A_2. This particular drive scheme preferentially excites rotational motion about the x axis. Hence, the unknown moment of inertia about this axis can be determined by comparing the measured transfer function with the theoretical transfer function. As was done in the unloaded case, the parameter value is determined which minimizes the error function between the measured and theoretical transfer functions.

The parameter identification procedure for the loaded case is an iterative procedure. The initial values for the unknown parameters are listed in table 2. The initial values for the spring stiffnesses and moments of inertia were taken from the results of the parameter identification for the unloaded system. Since the parameters L_7, L_8, and I_{xy} are not generally a priori known, they are initially set to zero. The initial value $L_9 = 0.08$ m was based on the known locations of

Test	Actuator	Displacement	Parameter Study				Figure
			Parameter	Initial Value	Final Value	Actual Value	
1	A_1+ A_3	z_2	L_7 (m)	0	-0.064	-0.075	--
2	A_1+ A_3	z_3	L_8(m)	0	0.048	0.075	--
3	A_1+ A_2+ A_3+ A_4	z_1	k_s (N/m)	11300	12100	--	8
4	(A_1+ A_2)- (A_3+ A_4)	z_3	$I_{xx}+I_{xx}^{e}$ (kgm^2)	0.340	0.433	0.455	9
5	(A_1+ A_4)- (A_2+ A_3)	z_2	$I_{yy}+I_{yy}^{e}$ (kgm^2)	0.259	0.278	0.374	10
6	A_1+ A_2	z_2	I_{xy}^{e} (kgm^2)	0	0.092	0.115	11
7	A_5+ A_7	x_3	$I_{zz}+I_{zz}^{e}$ (kgm^2) k_r (N/rad)	0.500 1590	0.752 1660	0.730 --	12
8	A_5+ A_8	x_1	k_t (N/m) L_9 (m)	37600 0.08	33300 0.117	-- 0.08	13

Table 2: Parameter identification results for the loaded vibration isolation system.

the load's *geometric* center and the unloaded plate's center of mass. Test cases 1-8 are sequentially handled, and the parameters determined at the end of each test case are used to update the model before considering the next test case. The procedure is continued until each parameter converges to within 5% of the value computed in the previous iteration. The parameters converged to the final results listed in table 2 after four iterations.

Table 2 also summarizes the actual values for the location of the load's center of mass and its products & moments of inertia. Overall agreement between the actual values and those obtained using the parameter identification procedure is good. Comparison between the measured and theoretical transfer functions are depicted in figs. 8-13 for selected test cases. The theoretical transfer functions were calculated using eqn. 32 and the final parameter set obtained from the parameter identification procedure. Overall agreement between experimental and theoretical curves is good. It is believed that the deviation between the curves at low frequency is caused by ground-induced motion of the lower plate and/or the limited low frequency response of the accelerometer. The deviation between the curves occurring at 40 Hz in figs. 8-11 is possibly caused by the vertical mounted resonant frequency of the vibration isolation system. This deviation is not present in the cases where the upper plate is horizontally driven (see figs. 12, 13), since the vertical mounted resonant frequency is only minimally excited/detected in these cases.

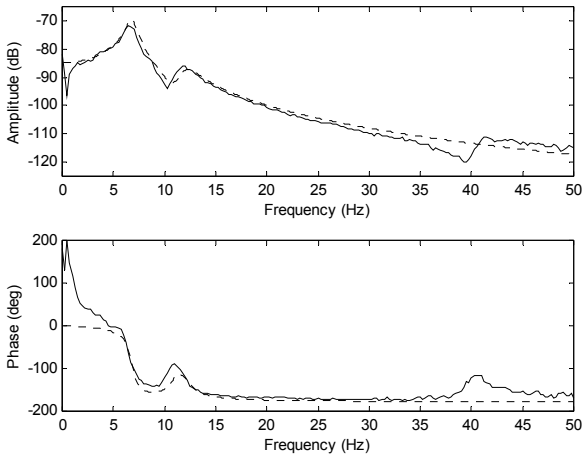

Fig. 8: Experimental (solid) and theoretical (dashed) Z_1/F_1 transfer functions for the loaded upper plate being driven by the $A_1+A_2+A_3+A_4$ actuator configuration.

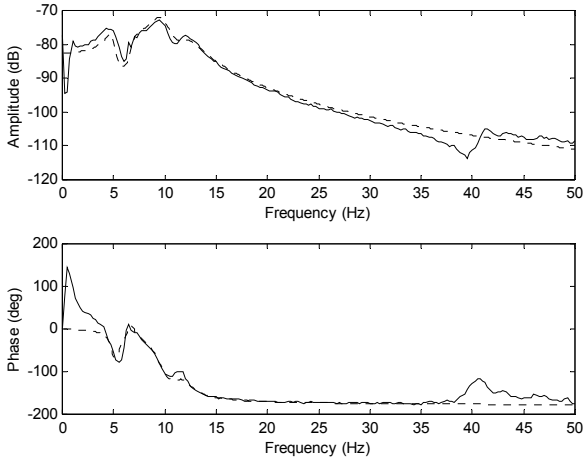

Fig. 9: Experimental (solid) and theoretical (dashed) Z_3/F_1 transfer functions for the loaded upper plate being driven by the (A_1+A_2)- (A_3+A_4) actuator configuration.

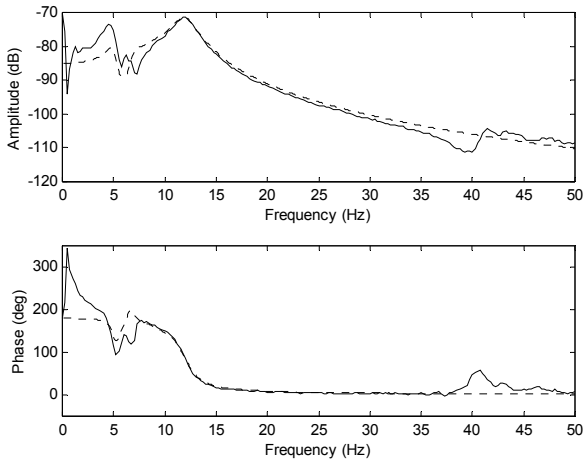

Fig. 10: Experimental (solid) and theoretical (dashed) Z_2/F_1 transfer functions for the loaded upper plate being driven by the (A_1+A_4)- (A_2+A_3) actuator configuration.

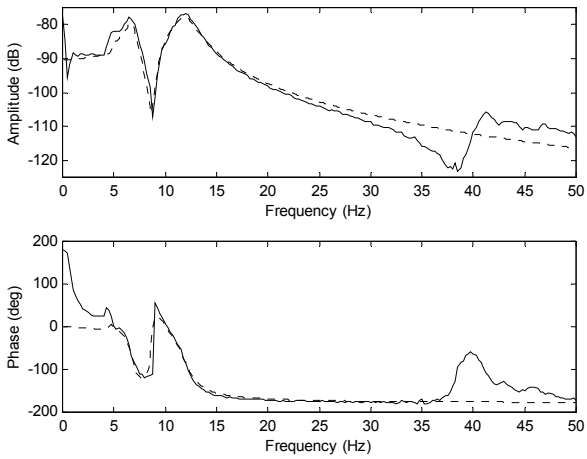

Fig. 11: Experimental (solid) and theoretical (dashed) Z_2/F_1 transfer functions for the loaded upper plate being driven by the A_1+A_2 actuator configuration.

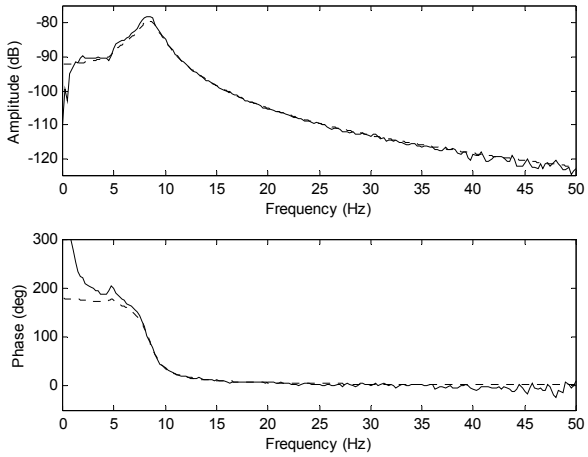

Fig. 12: Experimental (solid) and theoretical (dashed) X_3/F_5 transfer functions for the loaded upper plate being driven by the A_5+A_7 actuator configuration.

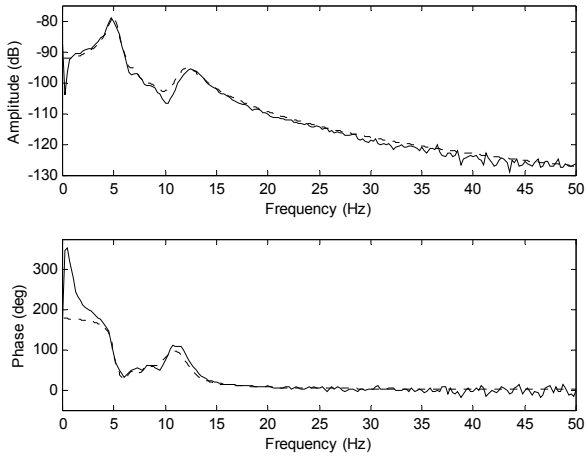

Fig. 13: Experimental (solid) and theoretical (dashed) X_1/F_5 transfer functions for the loaded upper plate being driven by the A_5+A_8 actuator configuration.

4. CONCLUSIONS

A six-DOF rigid body model for a commercially available vibration isolation system has been developed. The parameters of the unloaded vibration isolation system, including actuator transduction constants, spring stiffness, damping, moments of inertia, and the location of the center of mass, were determined by comparing measured transfer functions to those calculated using the updated model. The model was then re-updated for the case of an arbitrarily loaded system. The responses predicted by the final updated model agree well with the experimental measurements, thereby giving confidence in the model and the updating procedure. This work is important for model-based control techniques which require accurate identification of model parameters. Future work will involve construction of a test bed for driving the entire vibration isolation system in the vertical and horizontal directions. Various control concepts for minimizing the effect of the disturbance inputs, including adaptive and robust control algorithms, will be implemented and compared.

5. REFERENCES

[1] C.R. Fuller, S.J. Elliott, P.A. Nelson, *Active Control of Vibration*, Academic Press, 1996.

[2] U. Stöbener, L. Gaul, "Piezoelectric Stack Actuator: FE Modeling and Application for Vibration Isolation," *Proceedings of the NATO Advanced Study Institute on Responsive Systems for Active Vibration Control*, Ed. A. Preumont, Kluwer Academic Publishers, Dordecht, 2001.

[3] S. Hurlebaus, *Smart Structures- Fundamentals and Applications*, Lecture Notes, Institute A of Mechanics, University of Stuttgart, 2004.

[4] X. Huang, S.J. Elliott, M.J. Brennan, "Active Isolation of a Flexible Structure from Base Vibration," *Journal of Sound and Vibration*, **263**, 357-376.

[5] S. Riebe, H. Ulbrich, "Modeling and Online Computation of the Dynamics of a Parallel Kinematic with Six Degrees-of-Freedom," *Archive of Applied Mechanics*, **72**, 817-829, 2003.

[6] J.H. Ginsberg, *Advanced Engineering Dynamics, 2nd Ed.*, Cambridge University Press, New York, 1995.

[7] T. Müller, S. Hurlebaus, U. Stöbener, L. Gaul, "Modeling and Control techniques of an Active Vibration Isolation System," *International Modal Analysis Conference IMAC XXIII,* Orlando, 2005.